Chemistry–A European Journal
Research Article
doi.org/10.1002/chem.202404144
Chemistry Europe
European Chemical Societies Publishing
www.chemeurj.org

Technetium and Rhenium Auto-reduction, Polymerization and Lability towards Group VII Polyoxometalate Chemistry

Jenna Bustos,[a] Mohammad Shohel,[a] Ana Guilherme Buzanich,[b] Lev Zakharov,[a] Jordi Buils,[c, d] Mireia Segado-Centellas,[c] Carles Bo,[c, d] and May Nyman*[a]

Group VII Tc and Re have long been studied to develop both radiopharmaceuticals and technologies for nuclear materials management. Fundamental research has targeted understanding this periodic table crossroads where polyoxometalates meets metal-metal bonded complexes. Here we have isolated green hygroscopic and metastable crystals of $(Re^{VI,oct})_2(Re^{VII,tet})_2(OH)_2(O)_{12}{\cdot}H_2O$ (**$Re^{VI,VII}$-green**, *tet* = tetrahedral, *oct* = octahedral), determined by single-crystal x-ray diffraction. In addition to color, Re-L_1 X-ray absorption near-edge spectroscopy confirms the reduced oxidation state. **$Re^{VI,VII}$-green** provides the first demonstration of Re autoreduction, long-observed for Mn and Tc. We also isolated and structurally characterized $[Tc_4O_4(H_2O)_2(ReO_4)_{14}]^{2-}$ (**Tc_4Re_{14}**) polyanion crystals that contain Tc(V) and Re(VII), consistent with greater stability of reduced Tc compared to reduced Re. Small angle X-ray scattering of both compounds and prior-reported polyanion $[Tc_4O_4(H_2O)_2(TcO_4)_{14}]^{4-}$ (**Tc_{20}**) dissolved in acetonitrile indicated a qualitative lability order of oxo-linkages of Re-O–Re > Re-O–Tc > Tc-O–Tc, and lability of Tc_{20} was also probed by ^{99}Tc nuclear magnetic resonance spectroscopy. Computation provided insight into ^{99}Tc chemical shifts as well as lability. Based on both reducibility and solution phase dynamics of polynuclear compounds investigated here, Re is an imperfect surrogate for Tc, and further expansion of group VII polyoxometalate chemistry seems promising.

Introduction

Technetium-99 (a strong beta-emitter with a half-life of ~2.1×10^6 years) is one of the most problematic ^{235}U fission products that persists, migrates, and has unpredictable separations behaviour during nuclear fuel reprocessing and nuclear waste storage. Tc is abundant in legacy nuclear waste stored in tanks at the Hanford site.[1] In its most common and highest oxidation state (VII), Tc exists primarily as pertechnetate (TcO_4^-), which is water-soluble and highly mobile in aqueous environments. In addition to TcO_4^-, tank wastes contain reduced Tc species that presumably arise from the presence of organics and radiolysis.[2] Another concerning property of Tc^{VII} is the volatility of Tc_2O_7 (vaporization temperature ~300 °C), leading to airborne contamination that challenges high temperature processing (i.e. vitrification to prepare glass waste forms). In a very different application space, Tc-99m is the most commonly-used isotope for medical imaging,[3] but basic chemical research for developing Tc-radiopharmaceuticals must employ radioactive ^{99}Tc, given the ~6 hour half-life of the metastable isotope. Re is often utilized as a non-radioactive chemical surrogate for technetium due to their periodic relationship. Moreover, isotopes of rhenium are of interest in nuclear medicine where the β^- emitting ^{186}Re and ^{188}Re nuclides have properties suitable for radiopharmaceuticals.[4,5]

From a fundamental periodic table perspective, Tc and Re bridge the polyoxometalate (POM) forming metals of Groups V and VI (in their highest d^0 oxidation state), and the multiple metal-metal bonding Groups V through IX (in low oxidation states 2+ through 4+). Metal-metal bonding behaviour of groups V–IX leads to formation of dimers and small clusters, and this chemistry has been amply demonstrated since the 1960s.[6] Dimers and clusters exhibiting Re–Re and Tc–Tc bonding (usually 3+ oxidation state) are well-established in the literature, summarized and expanded in 2015.[7] On the other hand, identifying Tc and Re based POMs remains an intriguing challenge. In the 7+ oxidation state, the long-known M_2O_7 dimers and related compounds illustrate that polymerization is possible.[8,9] This behaviour was recently further demonstrated by a mass spectrometry study that identifies species up to Re^{VII}-oxo tetramers ($Re_4O_{15}^{2-}$), where the tetramer was crystallized.[10] Poineau[11] identified the major product of pertechnic acid autoreduction as a Tc isopolyanion formulated $[Tc_{20}O_{68}]^{4-}$ (Tc_{20}), later encountered as an ammonium salt through hydrolysis of a Tc^V complex $(NH_4)[TcO(OTf)_5]$ (Tf = triflate).[12] Tc_{20} features a $[Tc^V_4O_4]^{12+}$ central core, where each Tc^V is further decorated with four TcO_4^-. These two structures (Tc_{20} and Re_4) reported

[a] J. Bustos, Dr. M. Shohel, Dr. L. Zakharov, Dr. M. Nyman
Department of Chemistry
Oregon State University
Corvallis, OR 97331, USA
E-mail: may.nyman@oregonstate.edu
[b] Dr. A. G. Buzanich
Federal Institute for Materials Research and Testing (BAM)
Richard- Willstätter-Straße 11, 12489 Berlin (Germany)
[c] J. Buils, M. Segado-Centellas, Dr. C. Bo
Departament de Química Física i Inorgànica
Universitat Rovira i Virgili (URV)
C/ Marcel·lí Domingo s/n, 43007 Tarragona (Spain)
[d] J. Buils, Dr. C. Bo
Institute of Chemical Research of Catalonia (ICIQ)
Barcelona Institute of Science & Technology (BIST)
Av. Països Catalans, 16, 43007 Tarragona (Spain)
Supporting information for this article is available on the WWW under https://doi.org/10.1002/chem.202404144

within the last 3.5 years are rightfully described as the first group VII polyoxometalates, and they also highlight challenges in group VII POM chemistry. Specifically, in the highest oxidation state, corner-linking of polyhedra is favoured over the edge-sharing, the latter being the key feature that builds the stable cores of group V/VI POMs. We hypothesize that cation-cation repulsion of the highly-charged M^{VII} hinders edge-sharing, in addition to the preferred formation of three *cis*-M^{VII}=O double bonds,[12–14] limiting expansion of the coordination environment. Interestingly, Tc^{V} in Tc_{20} also exhibits only corner-sharing, despite possessing a charge and ionic radius comparable to POM-forming metals. Francesconi and coworkers have provided some of the most important advances towards group VII POM chemistry,[15–17] demonstrating the substitution of Tc^{V}=O into lacunary Wells-Dawson (α_2-$[P_2W_{17}O_{61}]^{10-}$) and Keggin ($XW_{12}O_{40}^{n-}$) polyoxometalates, in which the technetyl species is both octahedral and edge-sharing. Further, cyclic voltammetry illustrated reversible III/IV, IV/V and V/VI redox couples. We recently reported a heterometallic oxocluster featuring Tc^{V}=O square pyramid, edge-sharing with four uranyl pentagonal bipyramids.[18]

These examples of both pure group VII polyanions and heterometal oxoclusters and POMs provide inspiration to continue pushing the frontier of POM chemistry out to group VII. One synthetic strategy to diversifying POM chemistry is mixed metal POMs including W/Nb,[19] W/Ta,[20,21] Mo/W,[22] Nb/Mo,[23] Mo/Ta/W,[24] V/Nb,[25] where differences in preferred coordination geometry leads to new topologies and properties. With this inspiration, we have explored mixed pertechnetate/perrhenate chemistry, and an analogous auto-reduction study of perrhenate rounded out the present work. Evaporating a solution of mixed perrhenic/pertechnic acid yields $[H_3O]_2[Tc^{V}_4O_4(H_2O)_2(ReO_4)_{14}]\cdot 10H_2O$ (**Tc_4Re_{14}**), a derivative of Tc_{20}. Evaporating a solution of perrhenic acid yields mixed oxidation state **$Re^{VI,VII}$-green**, descriptively formulated $(Re^{VI,oct})_2(Re^{VII,tet})_2(OH)_2(O)_{12}\cdot H_2O$, as the first definitive example of Re^{VII} auto-reduction (*tet* = tetrahedral, *oct* = octahedral). Small-angle X-ray scattering (SAXS) of **Tc_{20}**, **Tc_4Re_{14}**, and **$Re^{VI,VII}$-green** in acetonitrile revealed higher lability of Re-O–Re linkages compared to Tc-O–Tc species, as observed prior in water for mixed actinide-perrhenate/pertechnetate coordination complexes.[18,26] Solution ^{99}Tc NMR characterization of Tc_{20} corroborates the lability of decorating TcO_4 ligands, and UV-vis spectroscopy verifies the existence of reduced Tc and Re, respectively for **Tc_4Re_{14}**, and **$Re^{VI,VII}$-green**. The oxidation state of **$Re^{VI,VII}$-green**, initially recognized by color, was also verified by Re L_1 XANES (X-ray absorption near edge spectroscopy), in addition to bond valence sum (BVS) calculations. Finally, ^{1}H NMR helped identify protonation of framework oxygens, needed for charge-balance and suspected by BVS calculations.

Results and Discussion

Synthesis and Characterization of $Re^{VI,VII}$-green and Tc_4Re_{14}

Evaporation of 100 μL of 0.5 M $HReO_4$ in an oxygen-free environment (details in SI) yields dark green, square, platy crystals (Figure S1) of **$Re^{VI,VII}$-green** (Figure 1). **$Re^{VI,VII}$-green** crystallizes in the tetragonal space group *$P4_2/ncm$* (Table S1). There are two crystallographically independent Re atoms, respectively a tetrahedral ReO_4^- and a distorted octahedral Re, which we eventually assigned as Re^{VI} based on various data (BVS data; Table S2, Figure S2). The ReO_6 octahedron bridges to four additional ReO_6 octahedra, one ReO_4^- tetrahedron, and a terminal oxygen (Figure 1c). The ReO_6 octahedra connect through corner sharing in the *ab* plane creating a layered structure. The corner sharing ReO_6 octahedra display bond lengths from 1.69(9) to 2.15(9) Å. Hydrogen bonding associates layers in the *c*–direction through interactions between the oxygens of ReO_4^- ligands and the lattice water molecule located in between the layers. The $O_{Re}\cdots O_{water}$ distance ranges from 2.82(2) to 2.86(2) Å, consistent with H-bonding distance. The ReO_4 has notable disorder, which is best modelled with partially occupied oxo-ligands.

Here it is worth comparing the structure of **$Re^{VI,VII}$-green** to prior-published Re_2O_7 (Figure S3).[27] Re_2O_7 features distorted squares of corner sharing and alternating $Re^{VII}O_6$ octahedra and $Re^{VII}O_4$ tetrahedra. The distorted squares are linked into an intricate net of corrugated double layers along the *ab* plane of the orthorhombic lattice. The interlayer space in the *c*-direction between the double layers is empty, with oxygen-oxygen distances around 3 Å, presumably associated only by dispersion forces. Notably, the **$Re^{VI,VII}$-green** square net of corner-sharing octahedra decorated with corner-linked tetrahedra resembles a polymerized Tc_{20}. An additional contrast between **$Re^{VI,VII}$-green** and prior-reported Re_2O_7 (and molecular $Re_2O_7(H_2O)_2$) is color.[27] While **$Re^{VI,VII}$-green** is forest green (Figure S1), anhydrous and hydrous rhenium (VII) oxides are respectively colorless and yellow.

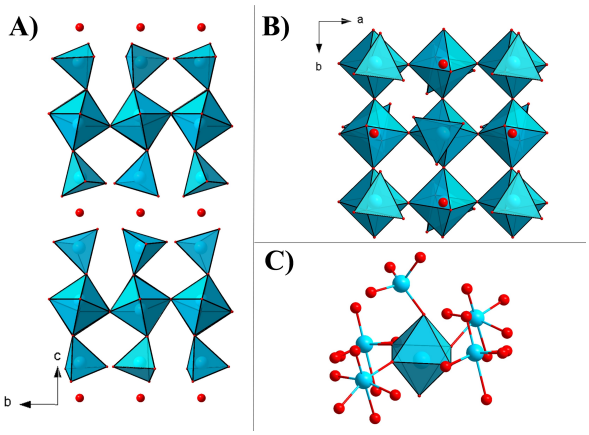

Figure 1. (A) **$Re^{VI,VII}$-green** layer stacking along, the *c*-direction, viewed along the *a*-axis. (B) View down the *c*-axis displaying the alternating bonding direction of ReO_4 tetrahedra and H_2O molecules in the *c*-direction. (C) Coordination environment of the Re- octahedral atom.

The isolation of **$Re^{VI,VII}$-green** demonstrates the periodic trend of Group VII metallic acids to autoreduce, also described by Latimer diagrams. For example, reduction potential from M^{VII} to $M^{IV}O_2$ becomes more negative from MnO_4^- (1.70 V) to TcO_4^- (0.75 V) to ReO_4^- (0.51 V).[28] Autoreduction and polymerization was first observed for Mn upon concentration of aqueous permanganic acid, which results in a violet colored $[Mn(MnO_4)_6]$[2] polyanion.[29] The Mn polyanion has a central Mn(IV) atom which coordinates to six MnO_4^- ligands through corner sharing. Similarly, concentration of pertechnic acid yields a red solution from which the Tc_{20} polyanion containing Tc^{V}[11] crystallizes. **$Re^{VI,VII}$-green** containing Re^{VI} obtained via $HReO_4^-$ (aq) evaporation is hygroscopic and unstable under ambient conditions. **$Re^{VI,VII}$-green** completes the trend of observed autoreduction of Group VII metallic acid, with a clear trend in reduction stability, observed qualitatively as $Mn^{IV} > Tc^{V} > Re^{VI}$.

While the green color indicates the presence of Re^{VI} based on prior studies,[30,31] more rigorous analysis was sought via XANES (X-ray absorption near-edge structure spectroscopy) at the Re L_1 edge (Figure 2). The mixed oxidation state is evidenced by 1) the pre-edge feature indicative of d^0 tetrahedral ReO_4^-, and 2) the white line energy of **$Re^{VI,VII}$-green** shifted to lower energy than the Re(VII) standard (tetrabutylammonium perrhenate, Table S3). For Re L_1 edge spectra, a shift to higher edge energy is typically observed with increased oxidation states.[31] Therefore, this shift to lower edge energy can account for a reduced species. To corroborate the oxidation state of the **$Re^{VI,VII}$-green** sample, we utilized an integral method[32–34] to determine the edge positions (details in SI). Edge energies were then correlated to formal oxidation state (Table S4, Figure S4).

Plotting the edge energies of the three standards with their respective oxidation states gives a linear fit for comparison to the unknown **$Re^{VI,VII}$-green**. This method yielded an average oxidation state of 6.32 for **$Re^{VI,VII}$-green** (Figure S3), in agreement with BVS analysis (Table S2, total avg oxidation state = 6.32). In sum, color (and UV-vis spectroscopy, discussed later), structure and XANES all evidence auto-reduction behavior of Re^{VII} to Re^{VI}.

The BVS calculations of the framework oxygens for **$Re^{VI,VII}$-green** vary from 1.297 to 2.125 (Table S2, Figure S2), where lower values could be OH^- instead of O^{2-}, and the isolated oxygen (O7) could be H_2O or H_3O^+. This needed to be considered for charge-balance, along with assigning Re oxidation state. We considered two possible formulations, both consistent with the BVS and XANES results: $(Re^{VI,oct})_1(Re^{VII,oct})_1(Re^{VII,tet})_2O_{14}{\cdot}H_3O^+$ vs. $(Re^{VI,oct})_2(Re^{VII,tet})_2(OH)_2(O)_{12}{\cdot}H_2O$, and ultimately discarded the former based on precedence and ^1H NMR experiments. **$Re^{VI,VII}$-green** dissolved in acetonitrile gave the ^1H NMR spectrum shown Figure S15. In addition to peaks arising from the acetonitrile peaks, we observe three downfield-shifted broad peaks at 8.10 ppm (major, plus a downfield shoulder), 8.54 ppm (minor), and 8.77 ppm (minor). This result is different than that observed for perrhenic acid in acetonitrile (Figure S15a), displaying peaks at 5.72 ppm, 5.99 ppm, and 6.10 ppm; meaning none of the observed peaks for dissolved **$Re^{VI,VII}$-green** represent perrhenic acid. To our knowledge, the ^1H NMR spectra of perrhenic and/or pertechnic acid have never been reported, and the origin of three peaks instead of one is certainly worthy of more indepth investigation in the future (but beyond the scope of the current study).

The peaks observed for **$Re^{VI,VII}$-green** are all consistent with proton NMR of OH^- bound to highly charged metals including Zr/Hf^{IV},[35] Nb^{IV},[36] W^{VI},[37] and Sb^{III}.[38] On the other hand, H_3O^+ in acetonitrile is reported at ~3 ppm.[39] Notably, the acetonitrile-dissolved species will not match the lattice, since SAXS evidences fragmentation, discussed later. We can further consider the low BVS values for O2 and O5, respectively 1.297 and 1.391 (Table S2) for assigning H_3O^+ vs. Re-OH for charge balance. Assigning both of these as OH^- and Re^{oct} as 6+ gives one extra positive charge per formula unit. Therefore we considered 'half OH, half O' for these two sites, where one is a disordered oxygen terminally bound to tetrahedral Re (Re2-O5~1.81 Å) and the other is disordered oxygen terminally bound to octahedral Re (Re1-O2~1.69 Å). Considering an O^{2-}/OH^- disorder (half for each) at these two sites would provide both charge balance and match the BVS. For example, Anderson et al. reported a 'half-protonated' bridging oxo site for a niobium POM, where the oxygen has a similar BVS of ~1.4.[40]

Evaporation of a 3:1 solution of $HReO_4$:$HTcO_4$ in an oxygen-free environment (details in SI) yields orange-brown platy crystals mixed with semi-solid of the same color (Figure S5, see SI for synthesis details). Based on solution analysis discussed below, we assume this non-crystalline substance also contains predominantly Tc_4Re_{14}, Tc_{20}, and perhaps other derivatives not yet confirmed. Tc_4Re_{14} crystallizes in the triclinic space group *P-1* (Table S1) and is fully formulated $[H_3O]_2[Tc_4O_4(H_2O)_2(ReO_4)_{14}]{\cdot}10H_2O$ (Figure 3 and S6). The polyanion has an inversion center, every atom in the cluster has a Wyckoff multiplicity of 2. Similar to prior-reported Tc_{20}, the polyanion consists of a $[Tc^{V}_4O_4]^{12+}$ core where the Tc oxidation state was confirmed by BVS (Table S5 & Figure S7). The four corner-sharing $Tc^{V}O_6$ octahedra feature Tc–O bond distances from 1.80(1) – 2.08(1) Å. The bridging ligands of the corner sharing octahedra are oxos, based on both their BVS > 2, and their nearly linear geometry (Tc-O–Tc ~170° and 175°). The $[Tc_4O_4]^{12+}$ unit is decorated by 14 ReO_4^- polyhedra via corner

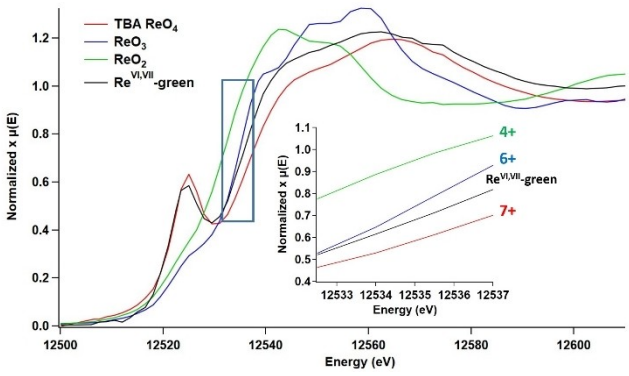

Figure 2. XANES spectra of Re L_1 edge for **$Re^{VI,VII}$-green** plus standards. The inset illustrates the area used for the integral method.

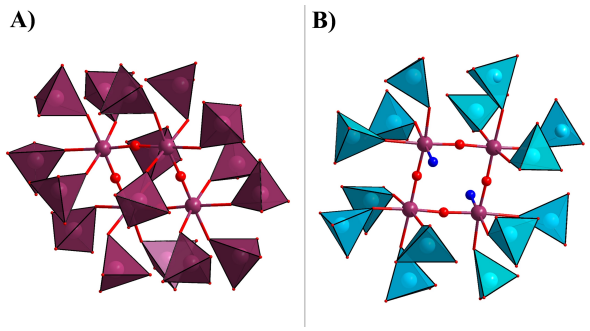

Figure 3. Prior-published[11] $[Tc_{20}O_{68}]^{4-}$ polyanion (A) compared to $[Tc_4O_4(H_2O)_2(ReO_4)_{14}]^{2-}$ polyanion (B) Purple is Tc, turquoise is Re, red is O, and dark blue is H_2O.

sharing. Similar to Tc_{20}, there is notable disorder amongst the tetrahedral (ReO_4^-) ligands. Per cluster unit, this was best modeled to include 1) two perrhenates with Re disordered over one half-occupied and two 1/4th occupied sites, and 2) six perrhenates with 1–3 terminal oxo-ligands disordered over two half-occupied sites (Figure S8). Per $[Tc^V_4O_4]^{12+}$ core, two Tc^V ions coordinate four ReO_4^-, and the other two coordinate three ReO_4^- and one terminal H_2O molecule (determined by BVS, Table S5). The replacement of two $M^{VII}O_4^-$ with water molecules is a departure from the Tc_{20} motif. Both the disorder in Tc_{20} and **Tc_4Re_{14}**, plus the two observed compositional variations suggests that everything from Tc_4 to Tc_4M_{16} (M=Tc, Re) could be isolated with tailored syntheses. A total of ten lattice oxygens (shown in Figure S6) were located, so we assume a formula that includes two charge-balancing hydronium ions and eight lattice H_2O molecules. **Tc_4Re_{14}** was crystallized from a very acidic media (perrhenic acid plus pertechnic acid), and no other charge-balancing cations are present that could serve as counterions. The location of the hydronium atoms within the unit cell cannot be determined crystallographically, and there is also disorder amongst the solvent molecules.

DFT calculations were performed to compared the favorability of capping the Tc_4O_4 core with ReO_4 vs. TcO_4 (Figure S9). This was done by calculating the energy to replace water ligands with the respective oxoanions.

$$Tc_4Tc_{14}(H_2O)_2 + 2TcO_4 \rightarrow Tc_4Tc_{16} + 2H_2O \; E = -8.97 \text{ kcal/mol}$$

$$Tc_4Re_{14}(H_2O)_2 + 2ReO_4 \rightarrow Tc_4Re_{16} + 2H_2O \; E = -12.57 \text{ kcal/mol}$$

These computational values suggest that the reaction involving the substitution of H_2O with ReO_4 is slightly favored to the substitution of H_2O with TcO_4, consistent with isolation of a ReO_4 capped Tc_4O_4 core from the mixed metal solution. However, the energies are similar, and we expect mixed TcO_4/ReO_4-capped clusters are possible.

The auto-reduction of Re and Tc in **$Re^{VI,VII}$-green** and **Tc_4Re_{14}/Tc_{20}** can be monitored by visible color change of the reaction solution from colorless to green and orange/brown, respectively. To directly compare solution behavior of Tc_4M_{16-x} (M=Tc, Re), we also prepared **Tc_{20}** (details in SI). To avoid reoxidation and disproportionation of the reduced species, the UV-vis absorbance spectra were obtained in acetonitrile (Figure 4), prepared in the oxygen-free glovebox. The UV-vis absorption spectrum of **Tc_{20}** in acetonitrile exhibits a broad band at 410 nm, a shoulder around 513 nm, and features at 260 and 222 nm. German *et. al*[11] reported a similar spectrum with a peak at 513 nm attributed to the excitation from occupied *d* orbitals of Tc(V) to empty *d* orbitals of neighboring Tc(V) atoms and also accounting for the red color, and a band at 407 nm accounting for the highest computed energy state based on time-dependent density functional theory (TD-DFT).[11] The spectrum of **Tc_4Re_{14}** in acetonitrile exhibits three bands at 230, 363, and 472 nm displaying similar features that are blue-shifted with respect to **Tc_{20}**. The band at 472 nm correlates to the *d-d* transitions seen at 513 nm in **Tc_{20}**, and the band at 363 nm correlates to *d-d* transitions observed at 410 in **Tc_{20}**.[11] The bands below 300 nm for both **Tc_{20}** and **Tc_4Re_{14}** can be attributed to ligand-to-metal charge transfer of the multiply-bonded oxos, expected at 230 nm for Re and 247 and 280 nm for Tc.[41] **$Re^{VI,VII}$-green** exhibits bands at 422 and 270 nm, with a small feature at 222 nm. The peak at 422 nm is in the same region described for Re(VI),[42] and the peaks below 300 is attributed to the above-described ligand-to-metal charge transfer.

SAXS Analysis of Tc_4Re_{14}, Tc_{20} and $Re^{VI,VII}$-green

Tc_{20} and **Tc_4Re_{14}** mixture of crystals and semi-solid material of the same color dissolved in acetonitrile both gave scattering curves (Figure 5) consistent with non-aggregating clusters; meaning the curves plateau at low q; ~ $q < 0.1$ Å^{-1}. The Guinier elbow (between $q = 0.1$ and $q = 0.4$ Å^{-1} for both **Tc_{20}** and **Tc_4Re_{14}**) gives the primary indication of cluster size. We both directly compared simulated scattering[43] from structural models to experimental data, and performed size analysis on the scattering curves. The experimental scattering of Tc_{20} best matched simulated Tc_{12}, with some decorating pertechnetate dissociated in solution (Figure 5a). Size distribution data fitting parameters for experimental Tc_{20-x} in acetonitrile and simulated

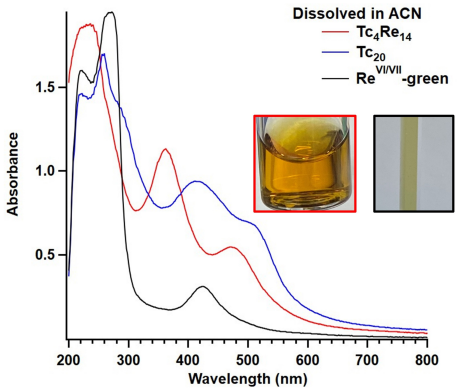

Figure 4. UV-vis spectra of **Tc_4Re_{14}** (red), **Tc_{20}** (blue), and **$Re^{VI,VII}$-green** (black) dissolved in ACN. The insets bordered in red and black display the colors of the Tc_4Re_{14} and **$Re^{VI,VII}$-green** solutions respectively in a vial and cuvette.

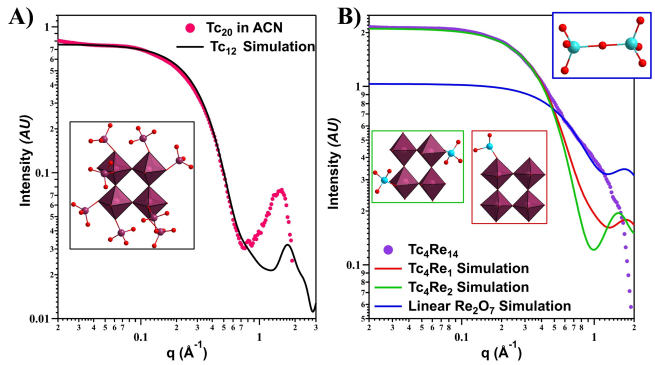

Figure 5. SAXS scattering curves of (a) **Tc_{20}** compared to a structural model of Tc_{12} and (b) **Tc_4Re_{14}** compared to models of Tc_4Re_1, Tc_4Re_2, and Re_2O_7.

Tc_{12} are summarized in Table S6 and Figures S10. The slight rise in scattering at q~0.03 $Å^{-1}$ indicates some aggregation of the clusters, and the disagreement between simulated and experimental scattering at $q > 1$ $Å^{-1}$ is attributed to solvent scattering. While simulated Tc_{12} scattering provides the best match to the experimental scattering data, other derivatives are likely present as well. Figure S11 illustrates a variety of hypothetical Tc_{20-x} species, plus their simulated scattering compared to the experimental scattering. While Tc_{20}, Tc_{16} and Tc_{12} all match the experimental scattering through the Guinier region, Tc_{12} provides a better agreement between maximum and minimum intensity (ΔI_q). Tc_{10}, Tc_6 and Tc_4 are smaller, with the Guinier elbow at higher-q.

Similarly, considering **Tc_4Re_{14-x}** derivatives, the experimental scattering best matches hypothetical Tc_4Re_1 and Tc_4Re_2 in the Guinier region (Table S6, Figure S12, Figure 5b, q~0.06-0.46 $Å^{-1}$). The notable increase in scattering intensity at $q > 0.5$ $Å^{-1}$ marks the presence of a second Guinier region, arising from a second population of smaller scatterers. We have observed this prior for Th-perrhenate solutions, and attributed it to free perrhenate in solution.[26] This would certainly be consistent with the identification of a smaller derivative of **Tc_4Re_{14}**; i.e. Tc_4Re_1 and Tc_4Re_2. However, a comparison of this second higher-q Guinier region (0.5 −1.5 $Å^{-1}$) to simulated ReO_4^- scattering indicates a larger species is present in acetonitrile solution. Given the growing knowledge about perrhenate/pertechnetate oligomerization, we considered several structures recently reported,[10] and found a linear Re_2O_7 provided the best match. Finally, we performed a two-phase fit on this scattering curve; the details are summarized in the SI and the results are summarized in Figure S13 and Table S7. The radius of Tc_4Re_x ($x = 1$-2) determined by size distribution agrees with that found in the two-phase fit. (Table S6 and Table S7).

SAXS analysis of **$Re^{VI,VII}$-green** dissolved in acetonitrile also produces a scattering curve consistent with non-aggregating species (Figure S14). Structural models were obtained from hypothetical fragments of the crystallographic structure of **$Re^{VI,VII}$**-green to compare the simulated scattering to the experimental scattering (Table S8). A radius of gyration (R_g, size independent root mean square average of scattering vectors from the center of the particle) of 2.54 Å was determined for the experimental scattering curve using the pair distance distribution function method of Moore (PDDF, Figure S15).[44] This best matches representative simulated scattering of various dimers and trimers, and suggests this loosely bonded framework dissociates to small mixed oligomers in solution. In summary, species size observed in ACN, based on comparing the R_g, trends Tc_{20} (5.93 Å) > Tc_4Re_{14} (4.91 Å) > $Re_2O_7{\cdot}H_3O^+$ (2.54 Å). This trend suggests Tc-O–Tc linkages are more robust than Tc-O–Re linkages, which are less labile than Re-O–Re linkages in polymerized oxides, and we expect higher stability in polymerized Tc-oxides in our quest for expanding Tc-POM chemistry.

^{99}Tc NMR Spectroscopy

^{99}Tc NMR of **Tc_{20}** dissolved in deuterated ACN (Figure 6) provided further insight into the possibility of a range of **Tc_{20-x}** compositions, wherein **Tc_{20}** is most readily crystallized. ^{99}Tc chemical shifts are predicted to range from~ +5000 to −3000 ppm relative to TcO_4^- (0 ppm), based on both computation[45] and experiment.[46] In addition, with a nuclear spin of $I = 9/2$ and asymmetric environments, we generally expect (and observe) very broad peaks.

The ACN solution of **Tc_{20}** initially exhibited a single broad peak centered at 21.4 ppm, which gradually narrows and shifts to 8.39 ppm (Figures 6 and S17). One interpretation is the broad peak represents free pertechnetate in exchange with bound pertechnetate initially. With time, it becomes dissociated. Based on both computation and experiment of prior-studied Tc(V) complexes, we expect ^{99}Tc peaks between +500 to +5000 ppm.[45,46] We do not observe a peak at or near this range, from scans between 5400 to 200 ppm. The putative peak for Tc_4O_4 could be broadened into the baseline, affected by 1) paramagnetic effects of the valence electrons, 2) asymmetry induced by lability of the decorating TcO_4^-, and 3) slow tumbling of the flat tetramer in solution. However, gradual transformation of bound to free TcO_4^- over 24 hours is consistent with the SAXS data.

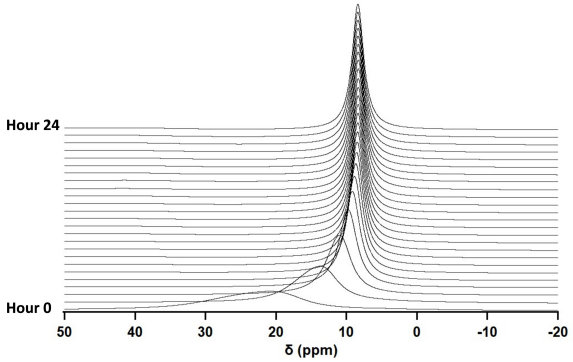

Figure 6. ^{99}Tc NMR of Tc_{20} dissolved in deuterated ACN, externally referenced to TcO_4^- (0 ppm).

Conclusions

Group VII polyoxometalate chemistry remains in its infancy, challenged by the polymerization behavior (linear, decorating) and restrictive coordination environments in the highest oxidation state. However, metastable pentavalent and hexavalent group VII metals exhibit more appropriate coordination environments. In this work, we demonstrate the auto-reduction ability of Re in acidic media through isolation of **$Re^{VI,VII}$-green**, well-known for the lighter congeners but not for rhenium. **$Re^{VI,VII}$-green** contains mixed Re^{VI}/Re^{VII} evidenced by color (and UV-vis), BVS and XANES analysis. Synthesis and characterization of **$Re^{VI,VII}$-green** completes the trend of auto reduction of group 7 metallic acids, observed in mixed oxidation state compounds ($Mn^{IV/VII}$,[29] $Tc^{V/VII}$,[11] $Re^{VI/VII}$). Combining perrhenic and pertechnic acids yielded the heterometal **Tc_4Re_{14}** polyoxometalate. Comparison of solution behavior by SAXS of **$Re^{VI,VII}$-green**, **Tc_4Re_{14}**, and **Tc_{20}**, revealed differences in lability, trending Re-O–Re > Tc-O–Re > Tc-O–Tc. These observations were highlighted by the solid-state isolation of **Tc_4Re_{14}** which is deficient of decorating tetrahedral ReO_4 (14 total) compared to Tc_{20} (16 total). In sum this work contributes to the understanding of fundamental group 7 redox and polymerization behavior, both important processes towards growing the nascent group 7 POM chemistry.

Acknowledgements

This study was primarily supported by the Department of Energy, National Nuclear Security Administration under award DE-NA0003763 (MN and Jenna Bustos). MN acknowledges the Alexander von Humboldt foundation for a research fellowship that supported the initiation of this project. Tc-99 was supplied by the U.S Department of Energy Isotope Program, managed by the Office of Isotope R&D and Production. We acknowledge the support of the Oregon State University NMR Facility funded in part by the National Institutes of Health, HEI Grant 1S10OD018518, and by the M.J Murdock Charitable Trust grant 2014162 for support of the SCXRD instrument. XANES experiments were performed at the BAM*line* at the BESSY-II storage ring (Helmholtz Center Berlin). We thank the Helmholtz-Zentrum Berlin für Materialien und Energie for the allocation of synchrotron radiation beamtime. JB (Jordi Bulis) and CB acknowledge the Spanish Ministry of Science, Innovation and Universities MCIN/AEI/10.13039/501100011033 (PID2023-153344NB–I00, and CEX2019-000925-S) and the ICIQ Foundation and the CERCA program of the Generalitat de Catalunya for the computational studies.

Conflict of Interests

The authors declare no conflict of interest.

Data Availability Statement

The data that support the findings of this study are available in the supplementary material of this article.

Keywords: Technetium · Polyoxometalate · Auto-reduction · Rhenium · SAXS

[1] R. Serne, B. Rapko, **2014**, No. PNNL-23319, EMSP-RPT-022, 1–146.
[2] S. Chatterjee, V. E. Holfeltz, G. B. Hall, I. E. Johnson, E. D. Walter, S. Lee, B. Reinhart, W. W. Lukens, N. P. MacHara, T. G. Levitskaia, *Anal. Chem.* **2020**, *92* (20), 13961–13970.
[3] A. Boschi, L. Uccelli, P. Martini, *Appl. Sci.* **2019**, *9* (12), 1–16.
[4] E. Deutsch, K. Libson, J. L. Vanderheyden, A. R. Ketring, H. R. Maxon, *Int. J. Radiat. Appl. Instrumentation.* **1986**, *13* (4), 465–477.
[5] S. Jurisson, D. Berning, W. Jia, D. Ma, *Chem. Rev.* **1993**, *93* (3), 1137–1156.
[6] F. A. Cotton, G. Wilkinson, *Advanced Inorganic Chemistry*, 5th ed.; **1988**.
[7] W. M. Kerlin, *Hydrothermal Routes to Technetium Cluster Compounds.* UNLV Theses, Diss. Prof. Pap. Capstones **2015**, 2485.
[8] D. S. Mast, K. V. Lawler, B. C. Childs, K. R. Czerwinski, A. P. Sattelberger, F. Poineau, P. M. Forster, *Inorg. Chem.* **2019**, *58* (9), 5468–5475.
[9] B. Krebs, H. H. Beyer, *Inorg. Chem.* **1969**, *8* (3), 436–443.
[10] M. A. Volkov, A. P. Novikov, N. E. Borisova, M. S. Grigoriev, K. E. German, *Inorg. Chem.* **2023**, *62*, 13485–13494.
[11] K. E. German, A. M. Fedoseev, M. S. Grigoriev, G. A. Kirakosyan, T. Dumas, C. Den Auwer, P. Moisy, K. V. Lawler, P. M. Forster, F. Poineau, *Chem. Eur. J.* **2021**, *27* (54), 13624–13631.
[12] M. Zegke, D. Grödler, M. Roca Jungfer, A. Haseloer, M. Kreuter, J. M. Neudörfl, T. Sittel, C. M. James, J. Rothe, M. Altmaier, A. Klein, M. Breugst, U. Abram, E. Strub, M. S. Wickleder, *Angew. Chemie - Int. Ed.* **2022**, *61* (3), e202113777.
[13] F. Poineau, P. F. Weck, K. German, A. Maruk, G. Kirakosyan, W. Lukens, D. B. Rego, A. P. Sattelberger, K. R. Czerwinski, *Dalt. Trans.* **2010**, *39* (37), 8616–8619.
[14] C. Soderquist, J. Weaver, H. Cho, B. McNamara, S. Sinkov, J. McCloy, *Inorg. Chem.* **2019**, *58* (20), 14015–14023.
[15] B. P. Burton-Pye, I. Radivojevic, D. McGregor, I. M. Mbomekalle, W. W. Lukens, L. C. Francesconi, *J. Am. Chem. Soc.* **2011**, *133* (46), 18802–18815.
[16] D. McGregor, B. P. Burton-Pye, R. C. Howell, I. M. Mbomekalle, W. W. Lukens, F. Bian, E. Mausolf, F. Poineau, K. R. Czerwinski, L. C. Francesconi, *Inorg. Chem.* **2011**, *50* (5), 1670–1681.
[17] I. Radivojevic Jovanovic, C. M. B. Gallagher, R. Salcedo, W. W. Lukens, B. P. Burton-Pye, D. McGregor, L. C. Francesconi, *Eur. J. Inorg. Chem.* **2020**, *2020* (22), 2133–2142.
[18] M. Shohel, M. Nyman, *Chem. Commun.* **2024**, 5820–5823.
[19] D. Zhang, Z. Liang, S. Xie, C. Zhang, J. Wang, J. Niu, *Inorg. Chem.* **2014**, *53* (18), 9917–9922.
[20] Q. Peng, S. Li, R. Wang, S. Liu, L. Xie, J. Zhai, J. Zhang, Q. Zhao, X. Chen, *Dalt. Trans.* **2017**, *46* (13), 4157–4160.
[21] P. I. Molina, D. J. Sures, P. Miró, L. N. Zakharov, M. Nyman, *Dalt. Trans.* **2015**, *44* (36), 15813–15822.
[22] C. Falaise, G. Mpacko Priso, N. Leclerc, M. Haouas, E. Cadot, *Inorg. Chem.* **2023**, *62* (6), 2494–2502.
[23] G. Zhang, E. Gadot, G. Gan-Or, M. Baranov, T. Tubul, A. Neyman, M. Li, A. Clotet, J. M. Poblet, P. Yin, I. A. Weinstock, *J. Am. Chem. Soc.* **2020**, *142* (16), 7295–7300.
[24] S. Li, G. Li, P. Ji, J. Zhang, S. Liu, J. Zhang, X. Chen, *ACS Appl. Mater. Interfaces* **2019**, *11* (46), 43287–43293.
[25] P. A. Abramov, A. T. Davletgildeeva, N. K. Moroz, N. B. Kompankov, B. Santiago-Schübel, M. N. Sokolov, *Inorg. Chem.* **2016**, *55* (24), 12807–12814.
[26] M. Shohel, J. Bustos, G. D. Stroscio, A. Sarkar, M. Nyman, *Inorg. Chem.* **2023**, *62*, 10450–10460.
[27] B. Krebs, H. H. Beyer, *Inorg. Chem.* **1969**, *8* (3), 436–443.
[28] M. Chotkowski, A. Czerwiński, Comprehensive Electrochemistry of Tc and Its Periodic Table Neighbors. In *Electrochemistry of Technetium*; Springer, 2021; pp 11–29.
[29] B. Krebs, K. D. Hasse, *Angew. Chemie - Int. Ed.* **1974**, *1* (13), 603.
[30] F. Ortega, M. T. Pope, *Inorg. Chem.* **1984**, *23*, 3292–3297.

[31] A. Tougerti, S. Cristol, E. Berrier, V. Briois, C. La Fontaine, F. Villain, Y. Joly, *Phys. Rev. B - Condens. Matter Mater. Phys.* **2012**, *85* (12), 125136.
[32] J. Dittmer, L. Iuzzolino, W. Dörner, H. F. Nolting, W. Meyer-Klaucke, H. Dau, *Photosynth. Mech. Eff.* **1998**, *II* (1), 1339–1342.
[33] H. Dau, L. Iuzzolino, J. Dittmer, *Biochim. Biophys. Acta - Bioenerg.* **2001**, *1503* (1–2), 24–39.
[34] H. Dau, P. Liebisch, M. Haumann, *Anal. Bioanal. Chem.* **2003**, *376* (5), 562–583.
[35] A. A. Roseborough, L. N. Zakharov, R. Loughran, C. A. Colla, M. Nyman, *Angew. Chemie - Int. Ed.* **2025**.
[36] M. Nyman, T. M. Alam, F. Bonhomme, M. A. Rodriguez, C. S. Frazer, *J. Clust. Sci.* **2006**, *17* (2), 197–219.
[37] Z. J. Berkson, M. Bernhardt, C. Copéret, *J. Phys. Chem. Lett.* **2024**, *15* (7), 1950–1955.
[38] Y. Watanabe, K. Hyeon-Deuk, T. Yamamoto, M. Yabuuchi, O. M. Karakulina, Y. Noda, T. Kurihara, I. Y. Chang, M. Higashi, O. Tomita, C. Tassel, D. Kato, J. Xia, T. Goto, C. M. Brown, Y. Shimoyama, N. Ogiwara, J. Hadermann, A. M. Abakumov, S. Uchida, R. Abe, H. Kageyama, *Sci. Adv.* **2022**, *8* (24).
[39] E. Alessandra Quadrelli, H. B. Kraatz, R. Poli, *Inorg. Chem.* **1996**, *35* (18), 5154–5162.
[40] T. M. Anderson, M. A. Rodriguez, F. Bonhomme, J. N. Bixler, T. M. Alam, M. Nyman, *Dalt. Trans.* **2007**, *9226* (40), 4517–4522.
[41] E. A. Katayev, G. V. Kolesnikov, J. L. Sessler, *Chem. Soc. Rev.* **2009**, *38* (6), 1572–1586.
[42] L. V. Borisova, A. N. Ermakov, Y. I. Plastinina, O. D. Prasolova, I. N. Marov, *Analyst* **1982**, *107* (1274), 500–504.
[43] R. Zhang, P. Thiyagarajan, D. M. Tiede, *J. Appl. Crystallogr.* **2000**, *33*, 565–568.
[44] P. B. Moore, *J. Appl. Crystallogr.* **1980**, *13* (2), 168–175.
[45] T. F. C. B. De Andrade, H. F. Dos Santos, C. Fonseca Guerra, D. F. S. Paschoal, *J. Phys. Chem. A* **2022**, *126* (32), 5434–5448.
[46] L. A. O'Connell, R. M. Pearlstein, A. Davison, J. R. Thornback, J. F. Kronauge, A. G. Jones, *Inorganica Chim. Acta* **1989**, *161* (1), 39–43.
[47] Deposition numbers 2391522 (for $\mathbf{Re_2O_7{\cdot}H_3O^+}$) and 2391523 (for $\mathbf{Tc_4Re_{14}}$) contain the supplementary crystallographic data for this paper. These data are provided free of charge by the joint Cambridge Crystallographic Data Centre and Fachinformationszentrum Karlsruhe Access Structures service.
[48] SAINT, version 8.34 A, Bruker AXS Inc., Madison, WI, **2013**.
[49] G. M. Sheldrick, *Bruker/Siemens Area Detector Absorption Correction Program*, Bruker AXS, Madison, WI, **1998**.
[50] G. Sheldrick, *Acta Cryst A* **2015**, *71*, 3–8.
[51] G. Sheldrick, *Acta Crystal A* **2008**, *64*, 112–122.
[52] O. V. Dolomanov, L. J. Bourhis, R. J. Gildea, J. A. K. Howard, H. Puschmann, *J. Appl. Cryst.* **2009**, *42*, 339–341.
[53] G. M. Sheldrick, *Acta Cryst. C* **2015**, *71*, 3–8.
[54] O. C. Gagne, F. C. Hawthorne, *Acta Cryst B* **2015**, *71*, 562–578.
[55] A. Guilherme Buzanich, M. Radtke, K. V. Yusenko, T. M. Stawski, A. Kulow, C. T. Cakir, B. Röder, C. Naese, R. Britzke, M. Sintschuk, F. Emmerling, *J. Chem. Phys.* **2023**, *158*, 244202.
[56] B. Ravel, M. Newsville, *J. Synchrotron Radiat.* **2005**, *12* (4), 537–541.
[57] D. W. Wester, N. J. Hess, *Inorganica. Chim. Acta* **2005**, *358*, 865–874.
[58] J. Ilavsky and P. R. Jemian, *J Appl Cryst* **2009**, *42*, 347–353.
[59] X. Zuo, G. Cui, K. M. Merz, L. Zhang, F. D. Lewis and D. M. Tiede, *PNAS* **2006**, *103*, 3534–3539.
[60] G. Te Velde, F. M. Bickelhaupt, E. J. Baerends, C. Fonseca Guerra, S. J. A. Van Gisbergen, J. G. Snijders, T. Ziegler, *J Comput Chem* **2001**, *22* (9), 931–967.
[61] M. Swart, A. W. Ehlers, K. Lammertsma, *Mol. Phys.* **2004**, *102*, 2467–2474.
[62] E. Van Lenthe, E. J. Baerends, *J Comput Chem* **2003**, *24*, 1142–1156.
[63] E. V. Lenthe, E. J. Baerends, J. G. Snijders, *J. Chem. Phys.* **1993**, *99*, 4597–4610.
[64] A. Klamt, *J. Phys. Chem.* **1995**, *99*, 2224–2235.
[65] M. Álvarez-Moreno, C. De Graaf, N. López, F. Maseras, J. M. Poblet, C. Bo, *J. Chem. Inf. Model.* **2015**, *55*, 95–103.

Manuscript received: November 10, 2024
Accepted manuscript online: February 20, 2025
Version of record online: March 4, 2025